From statics to dynamics: enhancing onshore velocity models with full waveform inversion

Terence Krishnasamy[1*], James Beck[1] and Cristina Reta-Tang[1] present an effective model-building workflow that incorporates FWI for both diving waves and reflections, utilising different cost functions.

Introduction

Near-surface characterisation plays a crucial role in accurately imaging deeper targets in onshore exploration seismic data. However, conventional model building techniques, such as reflection tomography, have limitations when it comes to updating near-surface velocities due to insufficient offset coverage at shallow depths. To overcome this, alternative methods like diving-wave or first arrival tomography have been widely used, offering updates to the shallow velocity model, albeit often lacking the necessary resolution.

In contrast, full waveform inversion (FWI) is a robust algorithm used to derive velocity models with high resolution and fidelity. FWI, based on direct solutions of the two-way wave equation, has been intensively developed in recent years because it provides a superior way to build high-resolution velocity fields, especially under complex geological settings. The inversion is performed by iteratively updating the model parameters by reducing the data differences between the observed and synthetic data. In recent years, it has been widely adopted in the industry, with successful examples of its application to marine data, especially for surveys acquired with rich azimuth long offsets and recorded with low frequency. However, onshore examples are not as abundant (Mei & Tong, 2015; Lemaistre et al., 2018; Tang et al., 2021; Masclet et al., 2021; Sheng et al., 2022, Krishnasamy et al., 2023).

There are several challenges for FWI in onshore applications. Onshore seismic data are acquired on non-flat datum (topography). As such, wavefield propagation from this non-flat surface must be addressed to achieve accurate results and be computationally efficient. Additionally, the low signal-to-noise ratio (SNR) of onshore data poses a challenge, mainly due to near-surface heterogeneity which results in strong near-surface scattering. Furthermore, recent successful applications of FWI to onshore data have shown that it remains a challenge to take full advantage of the recorded energy below 5 Hz due to the highly variable SNR, even with nonlinear sweeps starting as low as 2 Hz (Durussel et al., 2022). Lastly, the weathering layer (i.e., the layer at or near the surface, mostly made up of unconsolidated and heterogeneous material) results in strong elastic effects such as surface waves and converted waves, which are not accounted for during acoustic simulation. While one could utilise an elastic FWI workflow to address the elastic challenge, in practice it is still resource intensive, especially with very low shear velocities present in the model.

We have developed an effective model building workflow that incorporates FWI for both diving waves and reflections, utilising different cost functions. Figure 1 shows a conceptual representation of the workflow, which has been applied to many onshore surveys from a variety of geological settings. Thus far, the workflow produces geologically plausible and consistent models for data acquired with legacy/conventional onshore acquisition setups.

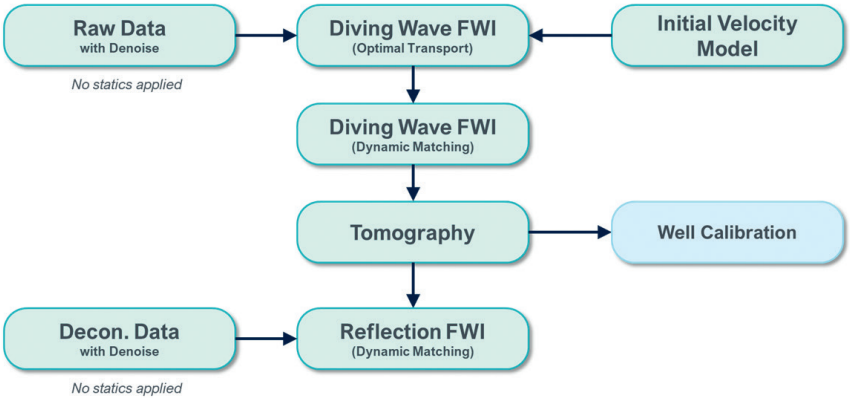

Figure 1 Conceptual representation of the FWI velocity model building workflow.

[1] TGS
[*] Corresponding author, E-mail: terence.krishnasamy@tgs.com
DOI: xxx

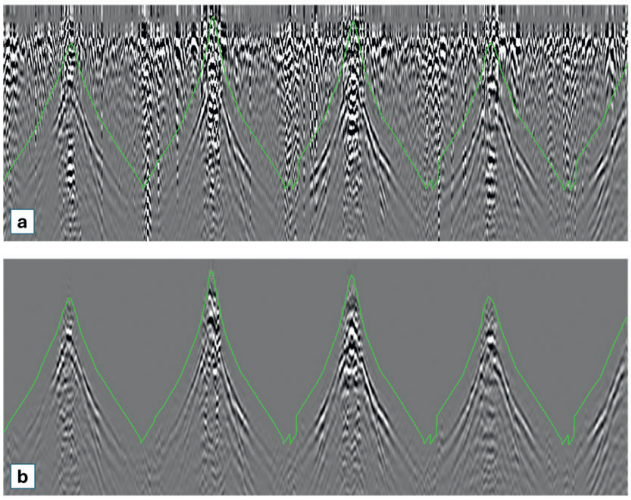

Figure 2 Example shot a) before pre-processing b) after pre-processing.

Initial near-surface model and pre-processing

The initial near-surface model was built using diving wave tomography and, where possible, supplemented by limited shallow sonic log information. Pre-processing the data to make it suitable for full waveform inversion (FWI) is an important step. The focus of this step is mainly to remove any unwanted energy that acoustic forward modelling is unable to capture, especially in the lower frequency ranges where the SNR is low. The steps include high amplitude noise suppression, ground-roll attenuation, inverse Q corrections, and surface consistent scaling. Figure 2 shows example shots before and after preprocessing. Despite these data preconditioning efforts, the usable starting frequency for the FWI is generally limited to around 5 Hz due to the variable SNR.

It is important to note that no statics correction, including any residual statics, was applied to the data used in the FWI workflow. Our results show that by not applying any residual statics to the data, we capture more details in the velocity model that would otherwise be captured by statics corrections. Typically, residual statics computed in time are based on normal moveout correction (NMO) velocities. NMO velocities assume the moveout is near hyperbolic in shape. However, in depth, when the velocity field is not the same, the vertical static corrections derived from the seismic weathering layer have little meaning to the depth migration process and begin to pull it away from accurately predicting geologic features. Figure 3 shows a synthetic data test on the effect of applying residual statics computed in time to a depth migration, taken from the study conducted by Ellison & Innanen (2016). In this study residual statics computed in time were applied to the input to the depth migration process. Comparing the resulting depth migrated images, the input data with residual statics computed in time have made the reflections less continuous compared to when no statics were applied to the input data.

Velocity model updates

FWI is a nonlinear inversion algorithm aimed at producing a velocity model that best explains the field data. This iterative algorithm involves forward modelling and migration of data residuals. The iteration stops when the synthetic shots sufficiently approximate the real data. It is then assumed that the resulting velocity model is a good estimate of the true model. Given the uncertainty in our initial velocity model (from refraction tomography) and limited starting frequency, diving wave FWI without cycle skipping was not initially possible. To overcome this, we utilised an optimal transport cost function using the quadratic Wasserstein distance (Engquist et al., 2016; Yang et al., 2018) that uses the trace envelope to compute the travel time information for the misfit. This cost function is less sensitive to the initial model. This approach allowed us to compute more robust travel time information for the misfit calculation and avoid cycle skipping, enabling us to update the low wavenumber background velocity model where low frequencies were deficient.

Having obtained a more accurate background velocity model, we transitioned to utilising a multi-channel dynamic matching (DMFWI) cost function, still focusing on the diving waves. The multi-channel DMFWI approach leverages normalised local window cross-correlations to quantify the time-dependent disparities between the observed and synthetic data (Mao et al., 2020; Sheng et al., 2020). This puts less weight on the amplitude discrepancy and focuses more on the kinematic difference between observed and synthetic data. Additionally, multi-channel windowing is used to mitigate the influence of noise in the input data. By doing so, we reduce the influence of noise and enhance the reliability of the inversion results. A multi-scale approach is also preferred, where the offset range and frequency bands used in the FWI updates are progressively increased. This helps to reduce the risk of cycle-skipping.

Diving wave penetration is usually limited on legacy/conventional onshore surveys. To update the deeper parts of the model where diving waves do not penetrate, we usually utilise reflection tomography. To capture and honor the velocity heterogeneity

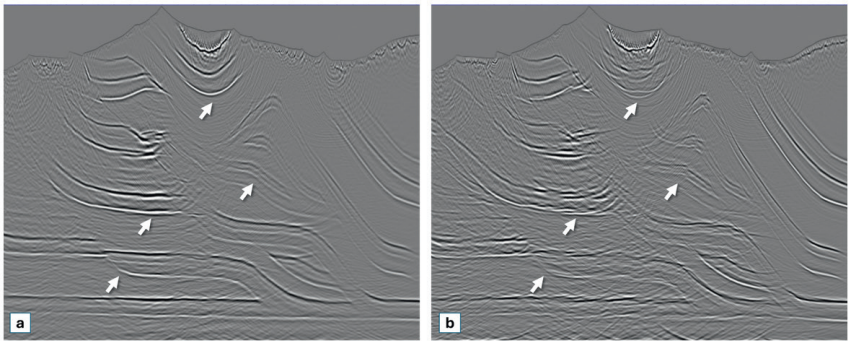

Figure 3 Depth migration of a synthetic dataset; a) with no residual statics and b) with residual statics from time. The arrows highlight areas where we see a significant degradation in the imaging when residual statics from time was applied (from Ellison & Innanen, 2016).

of the subsurface, multi-azimuth tomography updates were performed.

Subsequently, with this updated model, we continued the velocity model refinement using reflection FWI (RFWI) with the DMFWI cost function. At this stage of the processing, the input data has undergone further refinement. This includes surface consistent deconvolution, additional passes of noise attenuation (in different domains) and several passes of surface consistent scaling. To generate reflection events not present in the relatively smooth model obtained from diving wave FWI and reflection tomography, we introduced density contrasts using a pseudo-density model (Mao et al., 2019). This pseudo-density model is generated by migrating the input data at each RFWI iteration. This is then used to generate synthetic reflection events. Even though there may be errors in the velocity model, the near-angle times of reflection events will usually match up when comparing the actual data to the synthetic, due to the migration and de-migration effect. This will leave time differences at far angles for the RFWI to update the model with less chance of cycle-skipping. The frequency bands used in RFWI were progressively increased.

Case studies

The first data example is from an onshore survey conducted in East Texas, USA. The nominal source and receiver spacing is 50 m, with a source and receiver line spacing of approximately 300 m. This survey was acquired with mixed source types, dynamite and Vibroseis, with a nominal maximum offset of around 6000 m. To accurately process the data, different source wavelets were derived for each source type. Notably, up-hole corrections were not applied to the dynamite sources, which were buried at a nominal depth of 20 m. Instead, the shot depths were supplied to the FWI forward modelling so that it can be correctly accounted for during synthetic data generation.

Diving wave FWI started at 5 Hz, employing a multi-scale approach where the frequencies were progressively increased. This multi-scale strategy helps to mitigate the risk of cycle-skipping by gradually introducing higher frequencies, allowing the inversion to converge more reliably. Figure 4 compares the results of running diving wave FWI up to 15 Hz. When comparing the velocity model from refraction tomography with that from FWI (figures 4d and 4e), we can see that the velocity model from FWI was able to capture very shallow velocity anomalies in the study area. The resulting pre-stack depth migrated (PSDM) image, utilising the velocity model from FWI (Figure 4c), shows better event continuity and a more plausible geological structure.

With this improved velocity model from FWI, we recomputed surface-consistent mid- to long-wavelength statics and the corresponding surface consistent residual statics. Comparing the residual statics derived from long-wavelength statics using refraction tomography and the depth slice of the velocity model from FWI (Figures 5b and 5c), we observed a clear correlation between the anomalies identified by the FWI velocity model and higher statics values. This suggests that these anomalies would have been missed if residual statics were applied to our

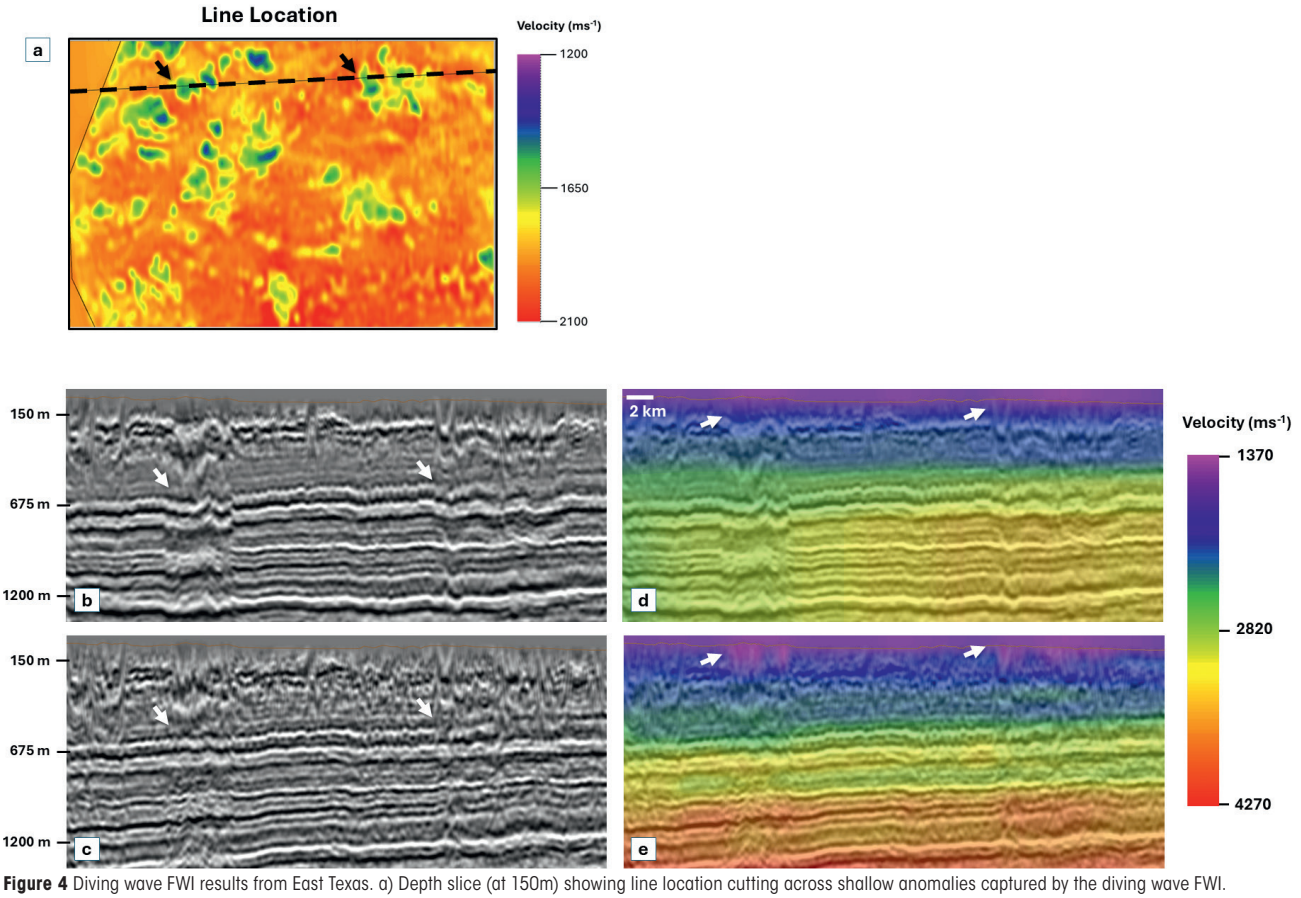

Figure 4 Diving wave FWI results from East Texas. a) Depth slice (at 150m) showing line location cutting across shallow anomalies captured by the diving wave FWI. b) Kirchhoff PSDM using the initial velocity model c) Kirchhoff PSDM using the velocity model after diving wave FWI; d) Initial velocity model; e) velocity model after diving wave FWI. The arrows show the distortion in the seismic image cause by the shallow anomalies and improvements brought by FWI.

input data. Furthermore, we can clearly see a reduction in the residual statics post-FWI (Figure 5d), indicating that the FWI process was able to recover some of the mid- to short-wavelength corrections from the residual statics and transfer that to a velocity correction.

The next study area comes from the Delaware Basin (a sub-basin within the Permian Basin) in Texas, USA. The Delaware basin is characterised by complex near-surface geology with shallow thick interbedded halite and anhydrite, resulting in a high velocity layered system. These sharp velocity contrasts limit diving wave penetration, and therefore applicability of diving wave FWI to update deeper events. The very shallow Rustler formation appears to collapse in some areas due to irregular evaporite dissolution below and is subsequently filled by much slower Cenozoic deposits creating a complex zone with high lateral velocity variations. This zone is commonly referred to as the fill zone. Figure 6 shows a geological cross section of the study area and a map of the extent of the fill zone. Historically, it has been difficult to image below the fill zone, where deeper events are distorted by those shallow lateral velocity changes. The nominal shot and receiver spacing for the data acquired in this study is 50 m, with source and receiver line spacing of 300 m, with a maximum offset of around 7000 m. The survey was acquired using Vibroseis sources exclusively, with a sweep that started at 2 Hz. However, as discussed earlier, the lowest usable frequency was only around 5 Hz.

We started the diving wave FWI using the optimal transport cost function. This allowed us to compute more robust travel time information for the misfit calculation and avoid cycle skipping so that we could update the low wavenumber background velocity model where low frequencies were deficient. Following this, we transitioned to utilising DMFWI to further refine the velocity model using the diving waves. A multi-scale approach was used in the DMFWI updates, and the frequencies were progressively increased to 12 Hz. Due to the limited penetration of diving waves into the halite and anhydrite layers, an additional tomography step was necessary. Subsequently, the model updating was continued using RFWI. The frequencies used for RFWI were progressively increased to 15 Hz.

We show the resulting Kirchhoff PSDM sections and corresponding velocity model at different stages in the FWI velocity model building process (Figure 7). The line shown cuts across

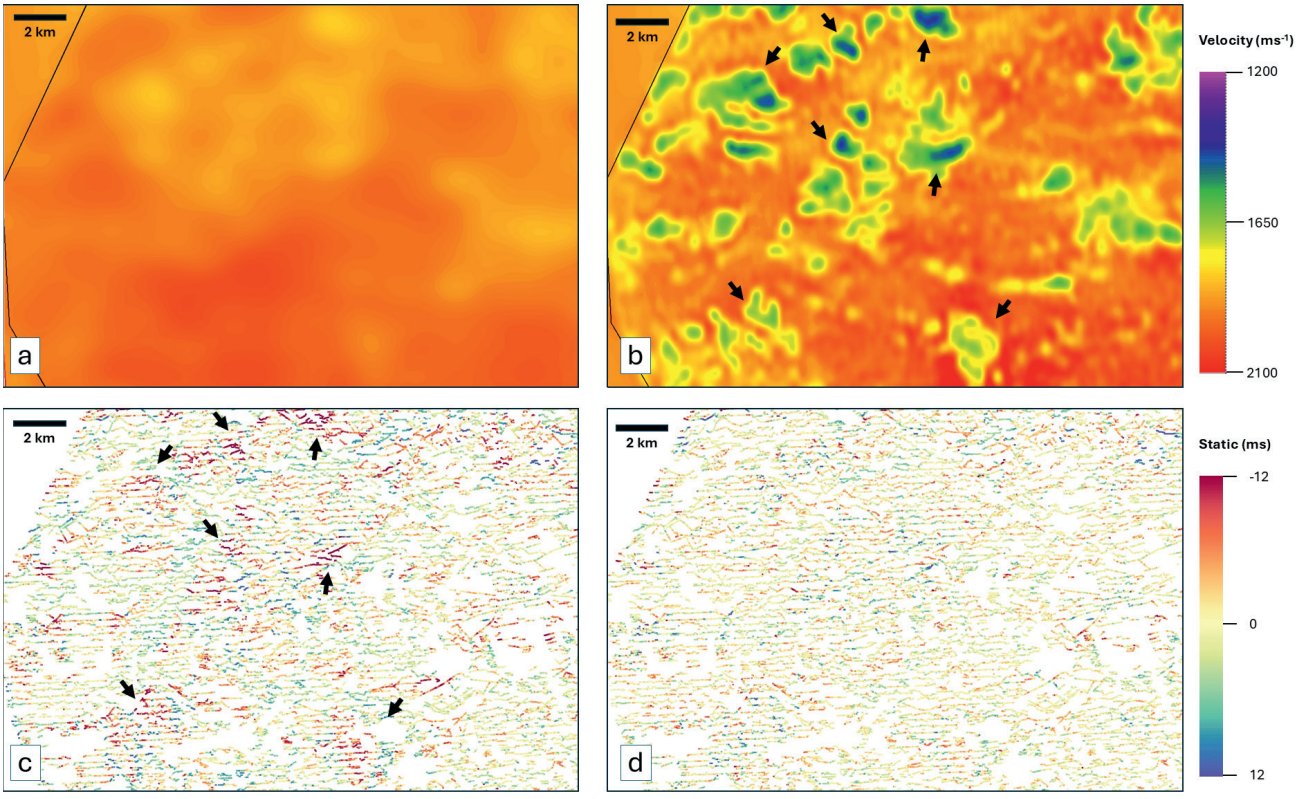

Figure 5 Depth slices at 150m a) initial velocity model; b) velocity model after diving wave FWI; c) residual statics map, based on refraction tomography, d) residual statics map, based on the velocity model from diving wave FWI. The arrows highlight areas where there is a correlation between the velocity anomalies captured in the FWI model and larger residual statics values.

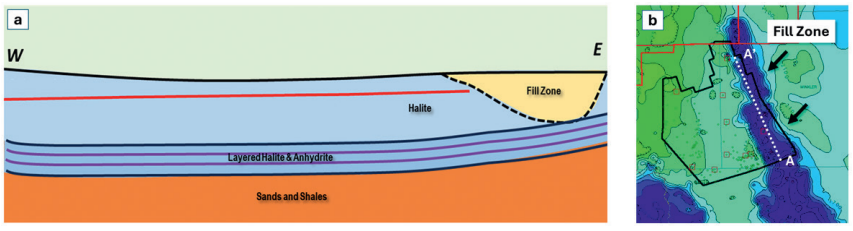

Figure 6 a) Geological cross section of the study area in the Delaware Basin. The Rustler formation is shown in red; b) area map showing the extent of the fill zone (in blue). The black polygon shows the extent of the study area.

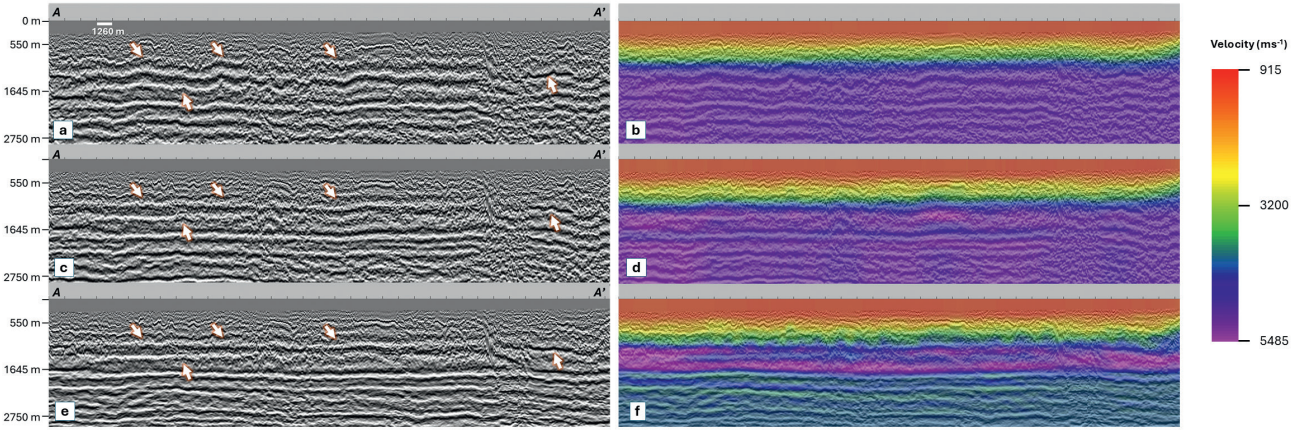

Figure 7 Kirchhoff PSDM and corresponding velocity model; a-b) after refraction tomography, initial model, c-d) after diving wave FWI, e-f) after reflection FWI. The arrows highlight areas where the seismic events show improvements after each stage of the velocity model updates using FWI.

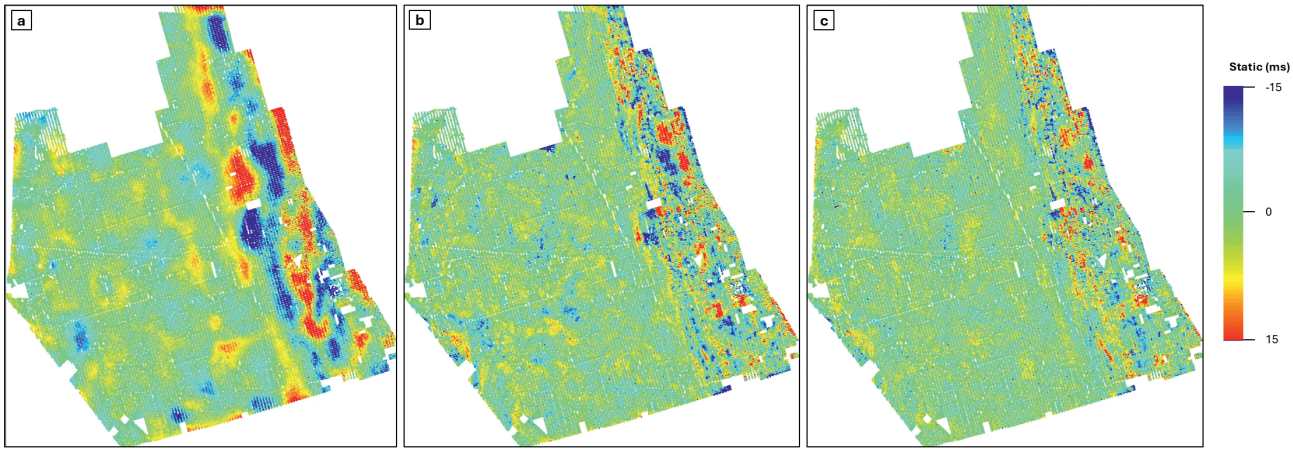

Figure 8 Surface consistent residual statics maps; a) computed after refraction tomography; b) computed after diving wave FWI; c) computed after reflection FWI.

the fill zone (line A - A' in Figure 6b). We can see that FWI progressively corrects for the extreme lateral velocity changes in this area, addressing the undulation present on the deeper events and improving their coherence. Residual statics were computed at different stages of the FWI velocity model updates and are compared in Figure 8. These comparisons show a progressive reduction in mid- to short- wavelength statics present in the residual statics at each stage of FWI. Suggesting that FWI recovered some of these static corrections and transferred them into a velocity correction at each stage.

Conclusion

The utilisation of FWI in these study areas presented several challenges that required careful consideration and strategic approaches. Our workflow was able to overcome these challenges, yielding velocity models that improve imaging quality. The successful application of our workflow to various onshore surveys, including challenging environments like the Delaware Basin, underscores its effectiveness.

We also show that it is possible to capture shorter wavelength corrections in onshore data using FWI, which are normally addressed by residual statics. This suggests that the approach of applying residual statics prior to FWI may not be the most effective strategy. Instead, allowing FWI to handle these corrections can lead to more accurate and detailed velocity models which might otherwise be obscured by the statics corrections.

References

Durussel, V., Bai, D., Ahmadi, A.B., Downie, S. and Mills, K. [2022]. The value of very low frequencies and far offsets for seismic data in the Permian Basin: Case study on a new dense survey from the Central Basin Platform: *The Leading Edge*, **41**(1), 34-39.

Ellison, D. and Innanen K. [2016]. Improved resolution in depth imaging through reflection statics corrections derived from model-based moveout. *CREWES Research Report*, **28**.

Engquist, B., Froese, B.D. and Yang, Y. [2016]. Optimal transport for seismic full waveform inversion. *Communications in Mathematical Sciences*, **14**, 2309-2330.

Lemaistre, L., Brunellière, J., Studer, F. and Rivera, C. [2018]. FWI on land seismic datasets with topography variations: Do we still need to pick first arrivals? *88th SEG Annual International Meeting*, Expanded Abstracts, 1078–1082,

Krishnasamy, T., Sheng, J., Florendo, R., Beck, J., Sierra, A., Murphy, S., Siebens, J. and Iwo-Brown, Y. [2023]. High-resolution near surface velocity model building across the Delaware basin Fill zone using FWI. *84th EAGE Annual Conference and Exhibition*, Extended Abstracts.

Mao, J., Sheng, J. and Hilburn, G. [2019]. Phase only reflection full-waveform inversion for high resolution model update. *89th SEG Annual International Meeting*, Expanded Abstracts, 1305–1309.

Mao J., Sheng, J., Huang, Y., Hao, F. and Liu, F. [2020]. Multi-channel dynamic matching full-waveform inversion. *90th SEG Annual International Meeting*, Expanded Abstracts, 666-670.

Masclet, S., Bouquard, G. and Prigent, H. [2021]. Multi-wave and full-waveform inversion in southern Oman. *82nd EAGE Annual Conference and Exhibition*, Extended Abstracts.

Mei, J. and Tong, Q. [2015]. A practical acoustic full waveform inversion workflow applied to a 3D land dynamite survey. *85th SEG Annual International Meeting,* Expanded Abstracts, 1220-1224.

Sheng, J., Mao, J., Liu, F. and Hart, M. [2020]. A robust phase-only reflection full waveform inversion with multi-channel local correlation and dynamic minimum total-variation constraint. *82nd EAGE Annual Conference & Exhibition*, Extended Abstracts.

Sheng, J., Reta-Tang, C., Liu, F., Vázquez Cantú, A. and Cabrales Vargas, A. [2022]. Full-waveform inversion and FWI imaging for land data. *Second International Meeting for Applied Geoscience & Energy*, 827-831.

Tang, Y., Gaines, D., Hefti, J., Every, Z., Neumann, E. and Pharis, R. [2021]. Land full-wavefield inversion for addressing complex near-surface challenges in the Delaware Basin. *First International Meeting for Applied Geoscience and Energy, SEG/AAPG*, Expanded Abstracts, 702-706.

Yang, Y., Engquist, B., Sun, J. and Hamfeldt, B. [2018]. Application of optimal transport and the quadratic Wasserstein metric to full-waveform inversion: *Geophysics*, **83**(1), R43–R62.